

## Article

# Effects of Mold Temperature on the Microstructures and Tensile Properties of the Thixoforged Graphite/AZ91D Composite

Kejian Geng<sup>1</sup>, Haipeng Jiang<sup>2</sup>, Suqing Zhang<sup>1,2,\*</sup>, Xin Gao<sup>1</sup>, Jianhua Wu<sup>1</sup>, Cuicui Sun<sup>1</sup>, Jixue Zhou<sup>1,\*</sup>  
and Xinfang Zhang<sup>1,3</sup>

<sup>1</sup> Key Laboratory of High Strength Lightweight Metallic Materials of Shandong Province, Advanced Materials Institute, Qilu University of Technology (Shandong Academy of Sciences), Jinan 250014, China; 17853465309@163.com (K.G.)

<sup>2</sup> Department of Mechanical and Electrical Engineering, Jining Polytechnic, Jining 272023, China

<sup>3</sup> School of Metallurgical and Ecological Engineering, University of Science and Technology Beijing, Beijing 100083, China

\* Correspondence: zhangsuqing@sdas.org (S.Z.); zhouxj@sdas.org (J.Z.)

**Abstract:** The effects of mold temperatures on the microstructures and mechanical properties of thixoforged Grp (graphite particles)/AZ91D composites have been investigated, followed by partial remelting and thixoforging technology. The results indicate that the best semi-solid microstructure could be obtained after being partially remelted at 600 °C and held for 60 min. Correspondingly, under a mold temperature of 300 °C, the best tensile properties were obtained by thixoforging. The UTS (ultimate tensile strength) and elongation of the thixoforged Grp/AZ91D were up to 304.1 MPa and 13.9%, respectively, which increased 11.3% and 43.1% in comparison with the thixoforged AZ91D, respectively. The variation of the tensile properties responded to the influences of mold temperatures on the amount of eutectic phase, the distribution of Grp, and the grain size of  $\alpha$ -Mg. Meanwhile, HRTEM (High Resolution Transmission Electron Microscope) showed good bonding between Grp and AZ91D, and many edge dislocations were found in the inverse FFT (Fast Fourier Transform) image. And the result showed that the increase in tensile properties is attributed to the synergistic effect of load transfer, dislocation strengthening, and Orowan looping mechanisms from the Grp strengthening the matrix.

**Keywords:** Grp/AZ91D composite; semi-solid microstructure; thixoforging; mechanical properties



**Citation:** Geng, K.; Jiang, H.; Zhang, S.; Gao, X.; Wu, J.; Sun, C.; Zhou, J.; Zhang, X. Effects of Mold Temperature on the Microstructures and Tensile Properties of the Thixoforged Graphite/AZ91D Composite. *Metals* **2023**, *13*, 1000. <https://doi.org/10.3390/met13051000>

Academic Editor: Atef Saad Hamada

Received: 24 April 2023

Revised: 18 May 2023

Accepted: 19 May 2023

Published: 21 May 2023



**Copyright:** © 2023 by the authors. Licensee MDPI, Basel, Switzerland. This article is an open access article distributed under the terms and conditions of the Creative Commons Attribution (CC BY) license (<https://creativecommons.org/licenses/by/4.0/>).

## 1. Introduction

Magnesium alloys have been widely used in electronic products and transportation, with high specific strength and low density [1–3]. However, magnesium still has some shortcomings in meeting some extreme conditions [4]. To further improve the properties of magnesium, the fabrication of MMCs (metal–matrix composites) is the most common method, of which SiC, TiC, Al<sub>2</sub>O<sub>3</sub>, and Mg<sub>2</sub>Si are the relatively common strengthening particles. Zhang fabricated Mg<sub>2</sub>Si<sub>p</sub>/AM60B by the thixoforging process, which improves the mechanical properties sharply [5]. Guan et al. prepared a SiC<sub>p</sub>-reinforced magnesium foundation matrix composite by stirring the casting process, and SiC<sub>p</sub> could be evenly distributed in the matrix and had good interface bonding. Simultaneously, the finer SiC<sub>p</sub> plays an important role in grain refinement [6]. Recently, carbon materials, such as grapheme, CNT (carbon nano tube) and graphite particles, reinforced MMC composites, have received attention in the research field [7]. Shahin et al. successfully prepared GNPs/Mg composites, where the addition of 0.30 wt.% could significantly improve the Young's modulus, tensile strength, and fracture strain (+131%, +49.5%, and +74.2%, respectively) [8]. Gao fabricated Grp/AZ91D composites by composite casting, which improved the hardness of the composites compared with the original alloy, and the distribution of Grp was determined by the self-stabilization mechanism [9]. Aatthisugan et al. prepared B<sub>4</sub>C-graphite/AZ91D hybrid

composites by stirring casting, which improved the strength, UTS, and wear-resistant properties of the composites [10].

Thixoforging is a relatively advanced method for fabricating Al and Mg components. The microstructures and the relevant tensile properties of the thixoforged components are determined by the technological parameters, particularly the mold temperatures, during thixoforging. Mold temperature affects the compactness of the secondary solidified structures and the amount of the eutectic  $\beta$  phases by changing the solidification rate, which then improves the tensile properties [11]. However, researchers' focus on this area is lacking in the published literature.

In this paper, the effects of mold temperature on the microstructure and tensile properties of thixoforged Grp/AZ91D composites have been systematically analyzed. Meanwhile, the interface structure and the strengthening mechanisms of the Grp have also been researched.

## 2. Experimental

### 2.1. As-Cast Preparation

Figure 1 illustrates the preparation process of the as-cast Grp/AZ91D. Commercial AZ91D ingots and self-made Grp/AZ91D pressed cakes were employed in this work. The detailed preparation process of those pressed cakes has been reported in the previous paper [9]. A quantity of the commercial AZ91D ingot (composition shown in Table 1) was melted in the furnace at 780 °C and refined with  $C_2Cl_6$ . Then a certain amount of Grp/AZ91D pressed cakes with an amount of Grp 1.5 wt.% were introduced in the melt with stirring for 3 min. After holding at 750 °C for 15 min, the melt was poured into the steel mold with a cavity of  $\Phi 50 \text{ mm} \times 350 \text{ mm}$ . The as-cast Grp/AZ91D composite ingots were obtained. It should be noted that the  $SF_6 + CO_2$  mixed gas was protecting the melt during the whole casting process.

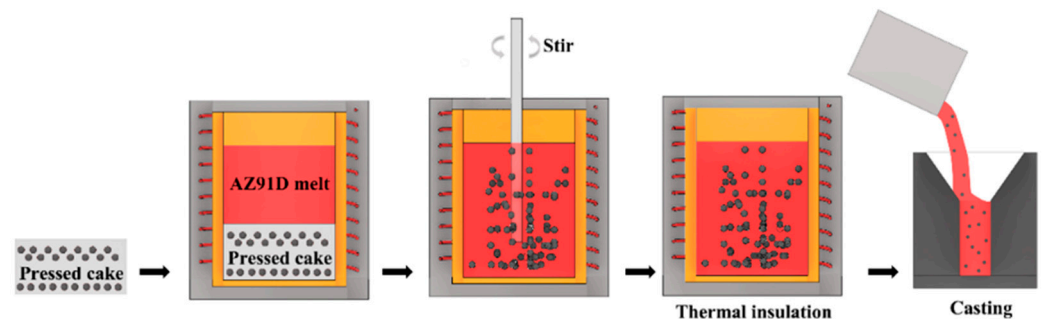


Figure 1. Schematic of as-cast preparation process.

Table 1. Element composition of AZ91D magnesium alloy (wt.%).

(wt.%)	Al	Zn	Mn	Si	Fe	Cu	Ni	Mg
AZ91D	8.5–9.5	0.45–0.90	0.12–0.4	0.05	0.004	0.025	0.001	Bal

### 2.2. Thixoforging Process

Some ingots with dimensions of  $\Phi 40 \text{ mm} \times 50 \text{ mm}$  were cut from the as-cast ingots. Then the ingots were held for 60 min under a semisolid temperature of 585, 590, 595, 600, 605, and 610 °C and protected by  $SF_6 + CO_2$  mixed gas. The preheating temperatures of the mold were 50, 100, 150, 200, 250, and 300 °C, respectively. Then the ingots were thixoforging at the applied punch velocity of 10 mm/s and solidifying at the applied punch pressure of 25 MPa. Meanwhile, the thixoforged Grp/AZ91D composite was prepared. The thixoforging process is schematized in Figure 2, and the technological parameters are shown in Table 2.

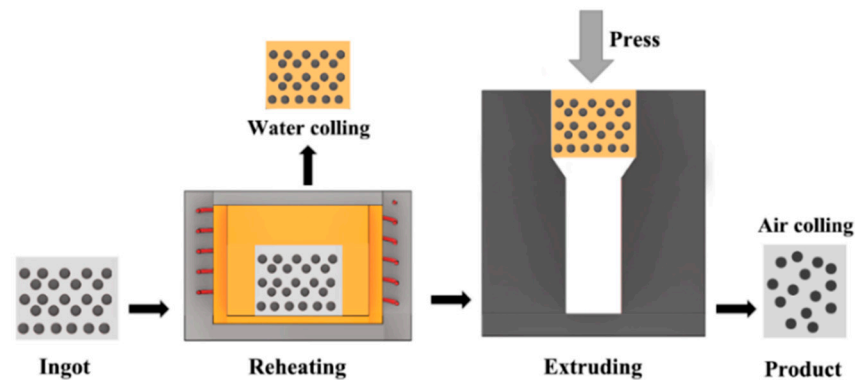


Figure 2. Schematic of thixoforming process.

Table 2. Parameters of thixoforming process.

Holding Temperature (°C)	Holding Time (min)	Mold Temperature (°C)			Protective Gas	Holding Time (s)
		50	150	250		
600	60	100	200	300	SF <sub>6</sub> + CO <sub>2</sub>	15
		50	150	250		

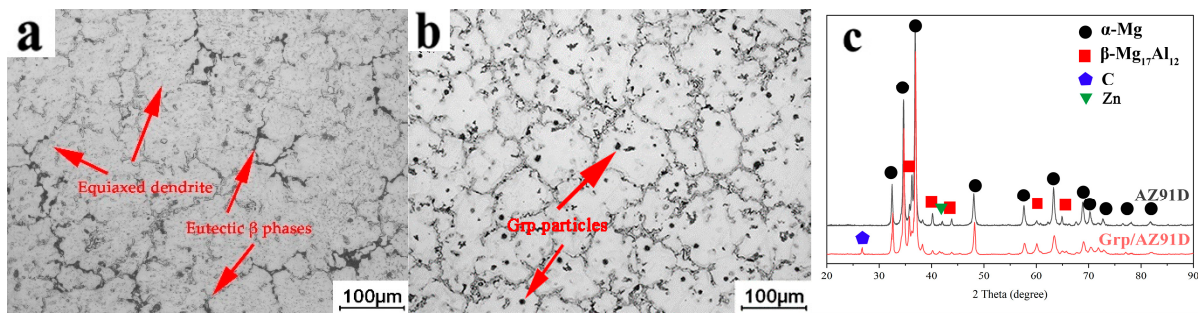
### 2.3. Microstructure and Tensile Analysis

The specimens for metallographic observation, which had a size of  $10 \times 10 \times 5 \text{ mm}^3$ , were cut from the center of the thixoforged Grp/AZ91D composite. The specimens were polished and etched with a 5 vol.% HNO<sub>3</sub> solution. The microstructure of the sample was observed by Optical microscope (OM, ZEISS, Oberkochen, Germany) and scanning electron microscope (SEM, Zeiss, Oberkochen, Germany). Subsequently, to analyze the specific phases of Grp/AZ91D composites and AZ91D ingots, a D/MAX-2500 X-ray diffractometer (XRD, Rigaku, Tokyo, Japan) was used. Then the composition was examined by EDS (Zeiss, Oberkochen, Germany) using a point scanning mode in the SEM. The microstructures of specimens were further analyzed by Image-Pro Plus 5.0 software (Image-Pro Plus 5.0, Media Cybernetics, Bethesda, MD, USA). The UTS of the materials was tested at a strain rate of 2 mm/s on a universal testing machine (MTS System (China) Corporation, Shanghai, China). Then, the fractographs were analyzed by OM and SEM as well.

## 3. Results and Discussion

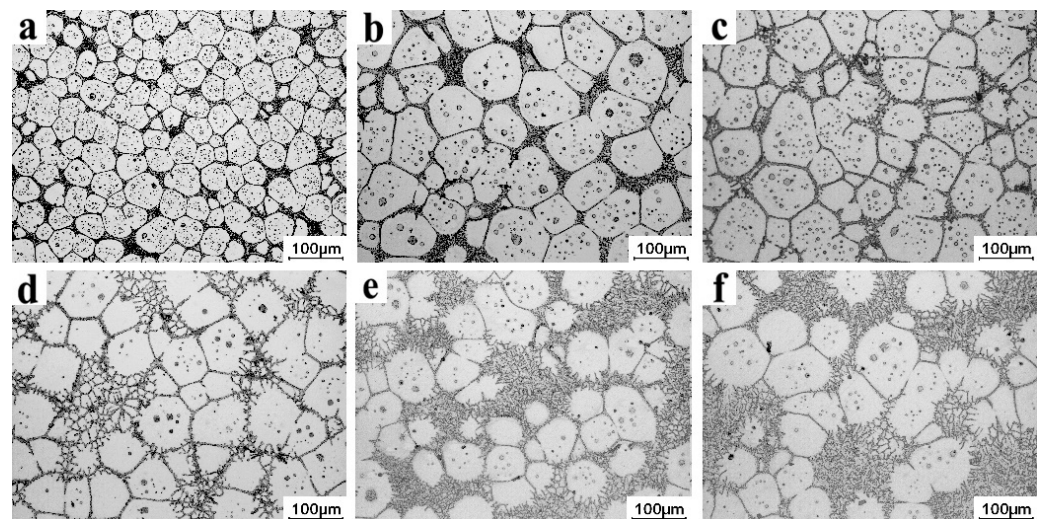
### 3.1. Effect of Holding Temperature on Semisolid Microstructures

Figure 3a,b shows that both the as-cast AZ91D and Grp/AZ91D composites are composed of fine equiaxed grains and inter-dendritic eutectic phases. Additionally, some dot-like particles (marked by arrows in Figure 3b) are uniformly distributed in the matrix of the as-cast Grp/AZ91D composites. Figure 3c shows the XRD results of the as-cast AZ91D and Grp/AZ91D composites. Both of them are composed of the  $\alpha$ -Mg phase and the  $\beta$ -Mg<sub>17</sub>Al<sub>12</sub> phase. In comparison, the C peak is detected in the as-cast Grp/AZ91D composite. Therefore, it should be inferred that the dot-like particles are Grp in the as-cast Grp/AZ91D composite.



**Figure 3.** Microstructure of (a) as-cast AZ91D; (b) as-cast Grp/AZ91D composite; and (c) XRD pattern.

The semisolid microstructures of Grp/AZ91D composites under different temperatures for 60 min are shown in Figure 4. The microstructures are composed of primary  $\alpha$ -Mg, Grp, and liquid phases. The fine primary  $\alpha$ -Mg particles are separated by the thin liquid layer under the holding temperature of 585 °C (Figure 4a). The fraction of the liquid phase is increased sharply in the holding temperature, the amount of intracrystalline liquid pools increases, and the grain size of primary  $\alpha$ -Mg particles first increases under 595 °C and then decreases (Figure 4b–f).



**Figure 4.** The semisolid microstructure of Grp/AZ91D under the holding temperature of (a) 585 °C, (b) 590 °C, (c) 595 °C, (d) 600 °C, (e) 605 °C, (f) 610 °C.

Figure 5 shows the variations of the primary  $\alpha$ -Mg particles, the shape fraction, and the liquid fraction in the semisolid microstructure with holding temperatures. It indicates that the shape fraction and size of primary  $\alpha$ -Mg first increase from 1.29 and 63.1  $\mu\text{m}$  to 2.53 and 124  $\mu\text{m}$ , respectively, with the holding temperature up to 595 °C, and then decrease to 1.1 and 98.1  $\mu\text{m}$ , respectively, with the temperature further increasing. However, when the temperature exceeds 605 °C, the shape fraction of primary particles decreases and the particle size increases.

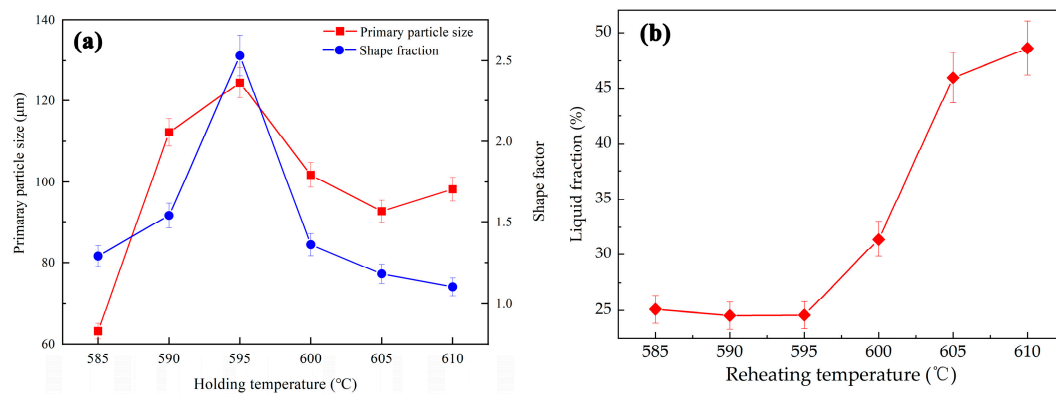


**Figure 5.** The variations of (a) the primary  $\alpha$ -Mg particle shape fraction and the size (b) liquid fraction with different holding temperatures.

When the holding temperature is below 595 °C, the liquid fraction is low (Figure 5b), and the primary  $\alpha$ -Mg particles are separated by thin liquid films. In this case, the particles are easier to contact with each other (Figure 4a,b). However, the energy of the semisolid system remains low, and the combination of the contacted primary particles is suppressed. The energy of the semisolid system increased with the increase in holding temperature. To reduce the solid–liquid interface energy, the contact or adjacent primary  $\alpha$ -Mg particles tend to be merged. Meanwhile, the atomic diffusion ability also increases with the holding temperature, which promotes particles to merge. Therefore, the size and shape fractions of grains increase sharply. However, when the holding temperature exceeds 600 °C, the liquid fraction increases sharply (Figure 5b), increasing the spacing between particles. Thus, the probability of merging is reduced. Simultaneously, the primary  $\alpha$ -Mg particles melt to liquid, and the particle size decreases (Figures 4d and 5a). With a further increase in temperature, the edges of polygonal particles melt first, which leads to the spheroidization of particles and an increase in the liquid fraction (Figures 4d–f and 5b). When the holding temperature reaches 605 °C, the atomic diffusion capacity is increased, and the structural evolution rate is accelerated too. The microstructure evolution of magnesium alloy during partial remelting can be divided into four stages sequentially: initial rapid coarsening, structure separation, spheroidization, and final coarsening [12]. When holding at higher semi-solid temperatures, the semi-solid microstructure enters the final coarse stage at an earlier time. As a result, the microstructures last longer under the Ostwald ripening mechanism [13], so the shape fraction decreases and the size of primary  $\alpha$ -Mg particles increases when the temperature exceeds 605 °C (Figure 5a).

According to the above discussion, the holding temperature affects the size and shape fraction of the primary  $\alpha$ -Mg and the liquid phase fraction. At temperatures below 600 °C, the primary  $\alpha$ -Mg with a smaller size can be obtained, causing a low content of the liquid phase and poor filling properties. When the holding temperature exceeds 600 °C, the grains begin to coarsen. Based on the above experimental results and previous research results on magnesium alloys [14], it is shown that an ideal semi-solid structure can be obtained when the holding temperature is 600 °C for 60 min. The appropriate semi-solid structure with grain size, shape fraction, and liquid fraction is 101.1  $\mu$ m, 1.36, and 31.3%, respectively.

### 3.2. Effect of Mold Temperature on Thixoforged Microstructure

The microstructure of thixoforged Grp/AZ91D composites under different mold temperatures is shown in Figure 6. All microstructures are composed of small dark Grp particles (red circles in Figure 6) and primary  $\alpha$ -Mg (bright regions in Figure 6). When the mold temperatures are below 100 °C, the secondary solidified structures (SSSs for short) are easily distinguished from the primary  $\alpha$ -Mg phase. Most of the Grp is distributed in the SSSs, and only a few Grp are distributed in the interior of primary  $\alpha$ -Mg particles (Figure 6a,b). With the further increase in mold temperature, the amount of SSSs seems to

decrease gradually, whereas more Grp is distributed inside the grain (Figure 6c). When the mold temperature reaches 300 °C, the grains contact each other, and the amount of SSSs seems to be further decreased.

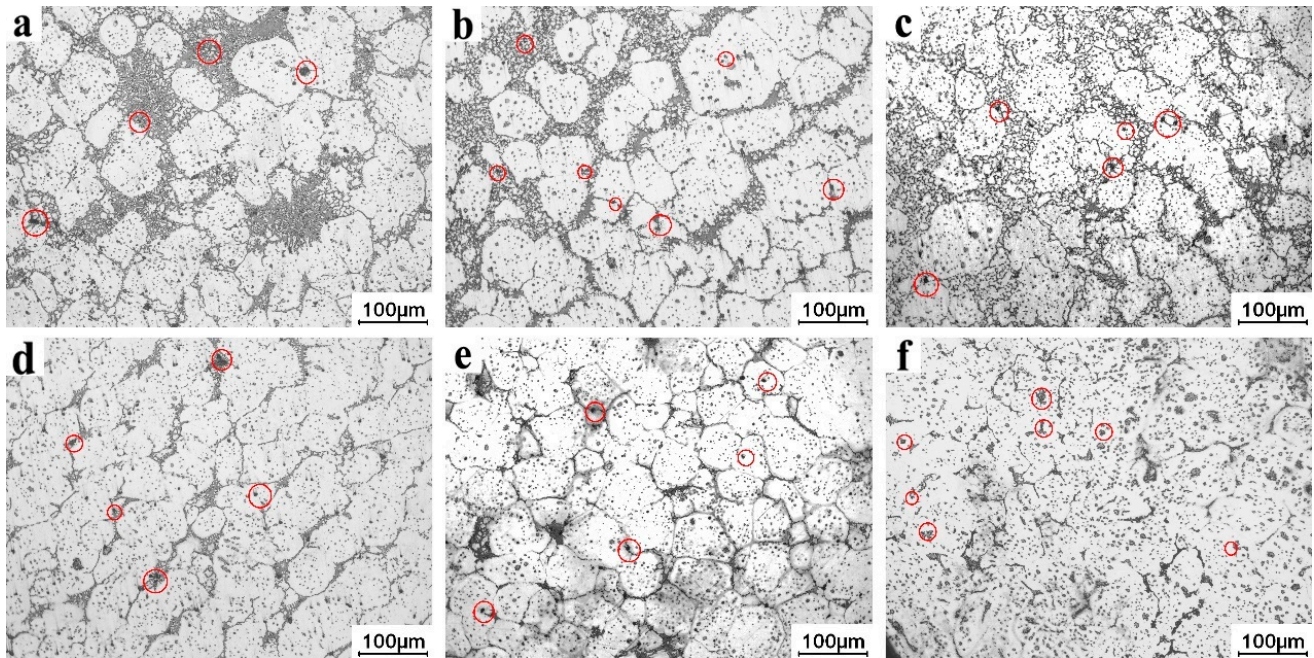


**Figure 6.** The microstructure of thixoforged Grp/AZ91D under different mold temperatures of (a) 50 °C, (b) 100 °C, (c) 150 °C, (d) 200 °C, (e) 250 °C, (f) 300 °C.

In the semi-solid microstructure, the liquid phase distributes around the primary  $\alpha$ -Mg particles, which act as the lubricant during the filling stage. Finally, the liquid phase solidifies into SSSs. Thus, it will be concluded that the amount of SSSs remains at a certain level, irrespective of the mold temperature. However, the experiment results contradict this inference. The following reasons are responsible for this phenomenon.

The first is that the solidified behavior changed as the mold temperature varied. It is well known that the solidification rate is closely related to the mold temperature. The liquid phase reaches the requirement of independent nucleation quicker under the lower mold temperature. As shown in Figures 6a and 7a, the liquid solidifies into SSSs surrounding the primary  $\alpha$ -Mg particles. The high mold temperature results in a low solidification rate. In other words, it is difficult for the liquid to solidify independently at a higher mold temperature. Therefore, the liquid directly grows up, attaching to the surface of the primary  $\alpha$ -Mg particles (Figures 6f and 7d). It is difficult to distinguish the primary  $\alpha$ -Mg particles from the SSSs, leading in the amount of SSSs seems to reduce.

The second reason results from the solidified rate as well. The lower the solidification rate, the more liquid is squeezed into the mold gap, resulting in a decrease in the amount of SSSs in the center region.

The third is that the composition changed as the mold temperature varied. Figure 7 shows the distribution of the  $\beta$  phases. It indicates that when the mold temperature is relatively low, a large amount of  $\beta$  phases are distributed in the matrix (Figure 7a). Increasing in the mold temperature, decreasing in the content of  $\beta$  phase. The net-like  $\beta$  phases transform into the dot-like phase, and the quantitative detection is shown in Figure 8. A decrease in the  $\beta$  phase content implies an increase in the secondary primary  $\alpha$ -Mg phases [11]. Furthermore, it could be expected that as the solidification rate decreased, more secondary primary  $\alpha$ -Mg phases are attached to the nucleation and growth of primary particles. In this case, the primary particles tend to be agglomerated and connected with each other. The content of each element in the magnesium matrix changes with the increase

in mold temperature (as shown in Table 3). The diffusion rate of the Al element accelerates with the increase in mold temperature, which mainly exists in  $\alpha$ -Mg phase in the form of a solid solution. When only two major elements (Al and Mg) are considered, from the Mg–Al equilibrium phase diagram, the Grp/AZ91D composite has a single  $\alpha$ -Mg phase interval under the solidification process [15].

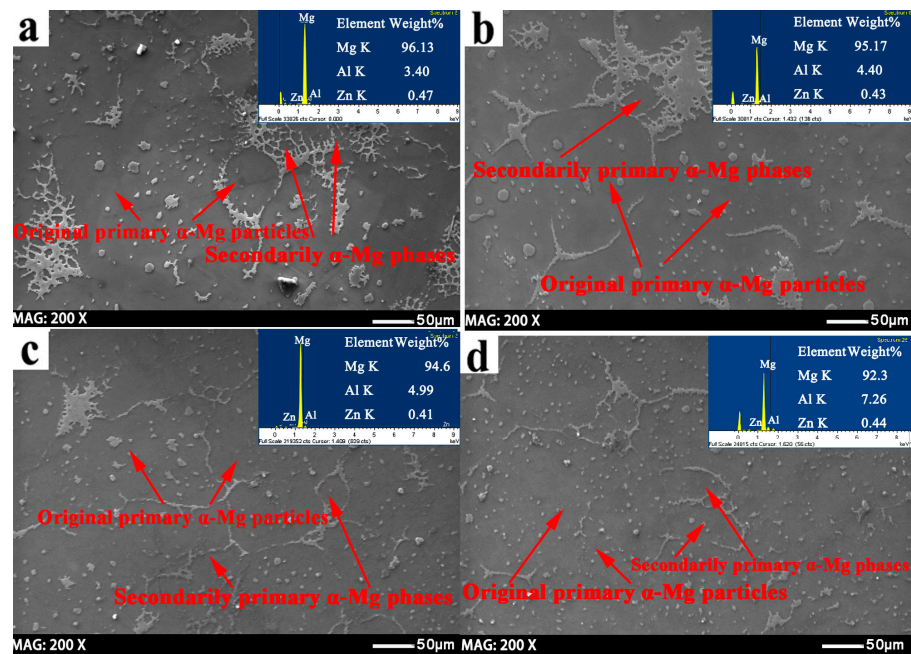


**Figure 7.** The SEM images of Grp/AZ91D under the mold temperature of (a) 50 °C, (b) 100 °C, (c) 200 °C, (d) 300 °C.

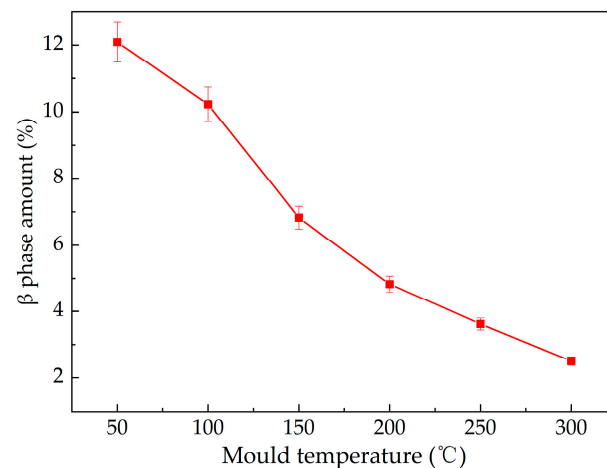


**Figure 8.** Variation in  $\beta$  phase content under different mold temperatures.

The distribution of Grp is also changing as the mold temperature varies. The Grp distributes in the SSSs regions at low mold temperatures and in the inner of the  $\alpha$ -Mg phases as the mold temperatures increase. The distribution of Grp is determined by the relationships between the front of the solidifying interface and Grp [16]. As mentioned above, at the low mold temperature, the solidification rate is quick. Thus, the Grp is pushed by the front of the solidifying interface to the last solidifying regions, which are the SSSs regions. With the increase in mold temperature, the system energy also increases, which makes it easier for Grp to be engulfed by the interface [16]. In this case, with the increase in mold temperature, Grp tends to distribute in the interior of grains.

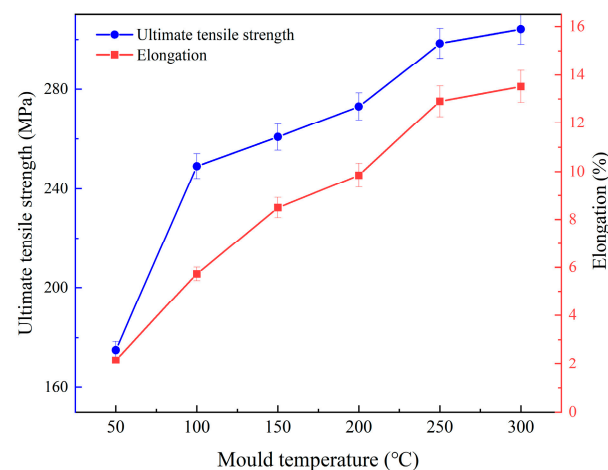
**Table 3.** Composition of  $\alpha$ -Mg phases of thixoforged Grp/AZ91D composites under different mold temperatures.

Mold Temperature (°C)	Compositions (wt.%)		
	Al	Zn	Mg
50	3.39	0.41	96.20
100	4.06	0.43	95.51
150	4.47	0.47	95.06
200	5.08	0.34	94.58
250	5.24	0.38	94.38
300	7.25	0.43	92.32

In conclusion, with the increase in mold temperature, the number of SSSs and  $\beta$  phases decreases. At the same time, the amount of Grp that distributes in SSS regions and grain boundaries reduces, and more Grp distributes in the interior of grains.

### 3.3. Effects of Mold Temperature on the Tensile Properties (UTS and Elongation) of Thixoforged Grp/AZ91D

Figure 9 shows the variations in UTS and elongation of thixoforged Grp/AZ91D composites with mold temperatures. It indicates that the UTS and elongation increase with an increase in mold temperature. Under the mold temperature of 300 °C, the maximum UTS and elongation are 304.1 MPa and 13.9%, respectively.

**Figure 9.** The variation in UTS of thixoforged Grp/AZ91D under different mold temperatures.

Figures 10 and 11 show the fractographs and a side view of them for thixoforged Grp/AZ91D composites with different mold temperatures. When the mold temperatures are between 50 °C and 100 °C, the tensile fractographs exhibit typical pore defect characteristics, which are caused by poor filling ability. At the low mold temperature, the liquid solidifies into the SSSs rapidly, and there is insufficient liquid phase to feed the last solidifying regions. Thus, the defects are easily formed in those regions, which are within the SSS regions. In this case, the cracks easily initiate in the SSSs and propagate along them (Figure 11a), i.e., the fracture mode of this composite belongs to the intergranular mode. Then the large-sized holes are formed on the fracture surface (Figure 10a,b), which correspond to the arrows A and B in the side view of the fracture surface (Figure 11a,b). The defects within the SSS regions, which are caused by the poor filling ability, are responsible for the low tensile properties under low mold temperatures.

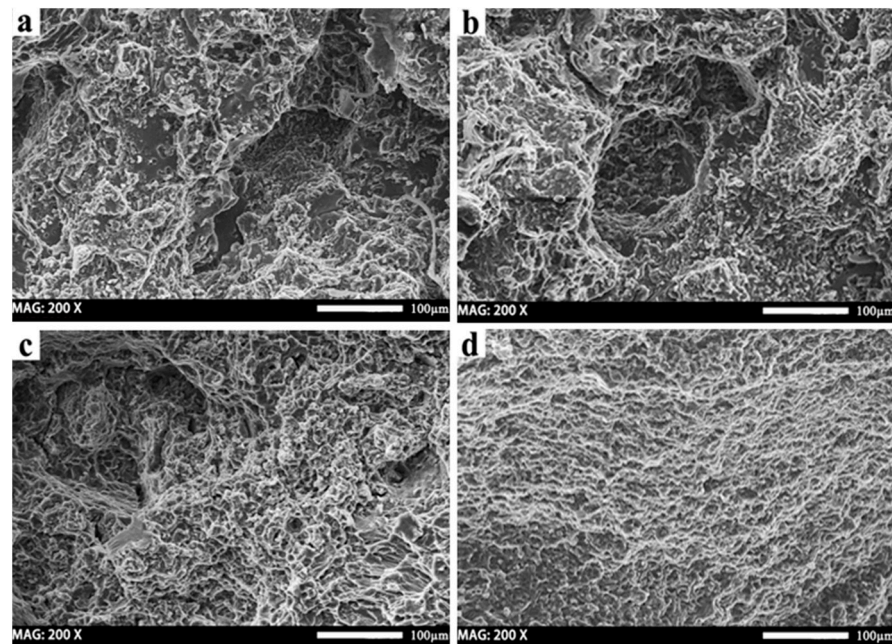


**Figure 10.** Fractographs of thixoforged Grp/AZ91D composites under the mold temperatures of (a) 50 °C, (b) 100 °C, (c) 200 °C, (d) 300 °C.

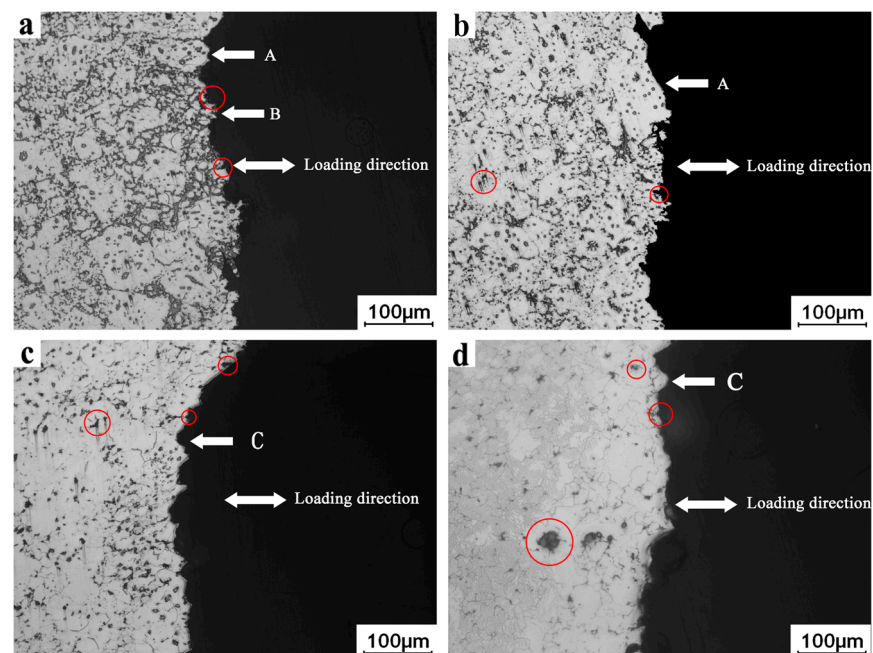


**Figure 11.** Fracture surface side views of thixoforged Grp/AZ91D composites under the mold temperatures of (a) 50 °C, (b) 100 °C, (c) 200 °C, (d) 300 °C.

Then, as the mold temperature increases gradually, the filling ability of the composite is enhanced, resulting in an improvement in the relative compactness of the SSSs. Figure 9 indicates that the tensile properties are gradually improving, and the pore characteristics on the fracture are gradually disappearing (Figure 10b–d). The fracture mode of the composite is transformed into transgranular and intergranular mixed modes. In addition, the reduction in the  $\beta$  phase also contributed to the improvement in tensile properties.

At the same time, with the increase in mold temperature, the amount of brittle eutectic  $\beta$  phase decreases, and the distribution region of Grp changes, which all affect the tensile

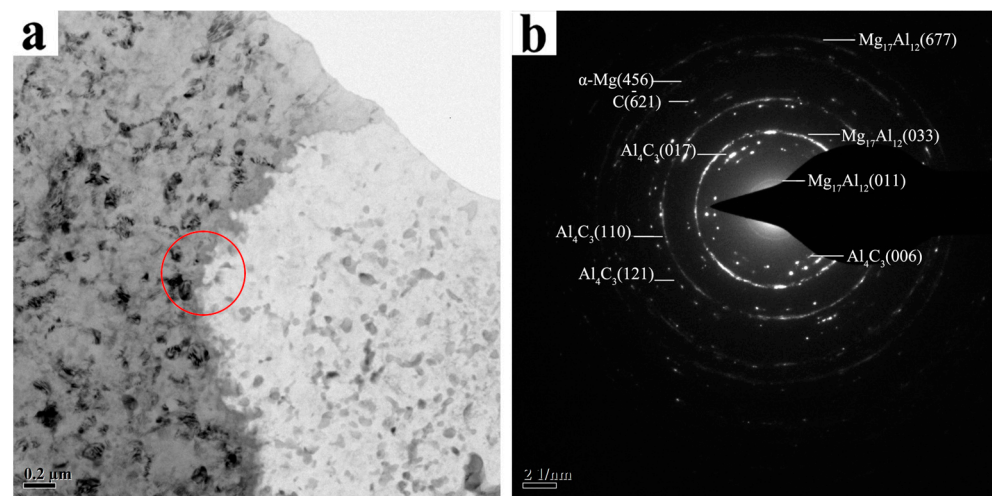
properties of the Grp/AZ91D composite. When the mold temperature is low, Grp is mainly distributed in the SSS area with many defects, resulting in a weak strengthening effect on the matrix. With the increase in mold temperature, the distribution of Grp tends to be inside the grain, and the strengthening effect on the matrix is enhanced. The specific strengthening mechanism of Grp on the matrix is discussed in the next section.

Based on the above discussions, the enhanced filling capacity results in an improvement in the compactness of the microstructure, which is the dominant reason for the excellent tensile properties of the thixoforged Grp/AZ91D composite under the high mold temperature. And the decrease in the  $\beta$  phases is a minor reason.

### 3.4. Strengthening Mechanisms of Grp for Thixoforged Grp/AZ91D Composite

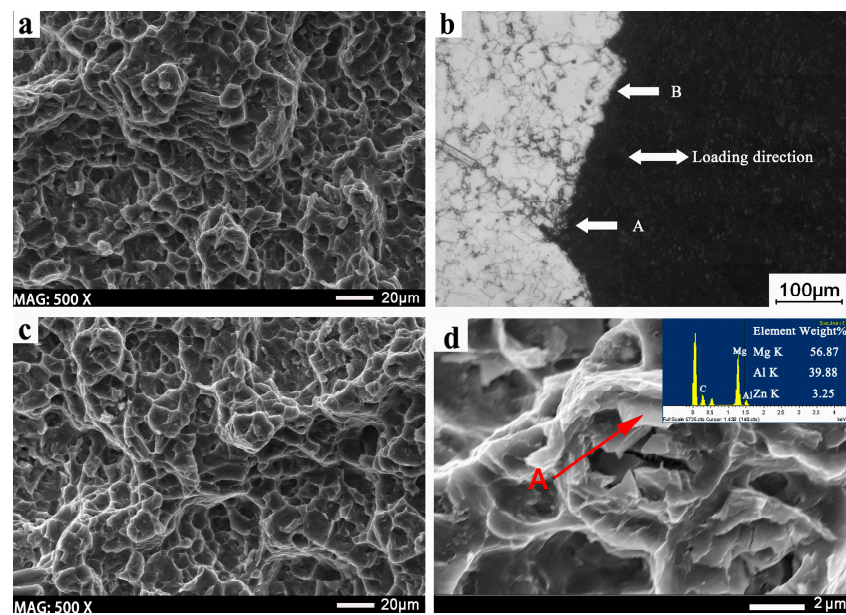
The UTS and elongation of the thixoforged Grp/AZ91D composite are 11.1% and 43.1% higher than the identical AZ91D alloys, respectively. The excellent tensile properties of the thixoforged Grp/AZ91D composite are attributed to the strengthening of the Grp.

Figure 12 indicates that the  $\text{Al}_4\text{C}_3$  is formed between the interface Grp/matrix. Therefore, the interfacial bonding strength of the Grp/matrix is high. According to the self-stabilizing effect of Grp and the solidification theory [17], Grp distributes dispersively, which improves the properties of the Grp/AZ91D composite by dispersion strengthening [9]. At the same time,  $\text{Al}_4\text{C}_3$  can be formed during the remelting process, which is shown in Figure 12.  $\text{Al}_4\text{C}_3$  can act as heterogeneous nucleation particles and refine the grains. The formation of the  $\text{Al}_4\text{C}_3$  phase can also inhibit the formation of  $\text{Mg}_{17}\text{Al}_{12}$  and enhance the mechanical properties to a certain extent [18].



**Figure 12.** TEM analysis images of Grp/AZ91D composites. (a) TEM brightfield images; (b) SAED pattern of interface region.

Figure 13a,b shows the fractography of thixoforged AZ91D; the morphology is mainly composed of cleavage steps, dimples, and tear edges. From side views of the fracture surface, the amount of  $\beta$  phase, which acts as the surface crack origin, is numerous. The cracks propagate along the  $\beta$  phase and lead to fracturing eventually. Figure 13c,d shows the fractography of thixoforged Grp/AZ91D composites. The morphology is mainly composed of dimples and tearing edges. The amount of  $\beta$  phase is less than that of thixoforged AZ91D, which indicates that the Grp can enhance the mechanical properties of AZ91D. EDS analysis of point A of the lamellar structure tissue in Figure 13d shows that element C is 56.8 wt.%. The analyses show that the size of the lamellar structure of the exposed film is 4–5  $\mu\text{m}$ , which is consistent with the size of Grp used in the work. Therefore, the load transfer mechanism is one of the important strengthening mechanisms for Grp to strengthen the matrix.



**Figure 13.** Fractographs of thixoforged composites (a) the fractograph of thixoforged AZ91D (b) the fracture side view of thixoforged AZ91D (c) the fractograph of thixoforged Grp/AZ91D (d) the EDS result at point A.

Meanwhile, the dislocation-strengthening mechanism also plays a role. The thermal expansion coefficients of Grp and magnesium are quite different (Grp:  $1 \times 10^{-6} \cdot \text{K}^{-1}$ , Mg:  $2.5 \times 10^{-5} \cdot \text{K}^{-1}$ ). As a result, many dislocations are formed around the Grp. Under the action of stress, dislocations expand in multiple directions and slip. Micron-scale Grp can hinder the progress of slip and deformation, which improves the strength of composites [19,20].

Figure 14a shows a clean interface between Grp and the AZ91D matrix, which indicates good bonding between them. Figure 14b shows the inverse FFT image of the interface, in which the crystalline features are clearly visible. In addition, many edge dislocations are observed, which can effectively improve the mechanical properties of composites (the position and direction of dislocations are identified by yellow T).

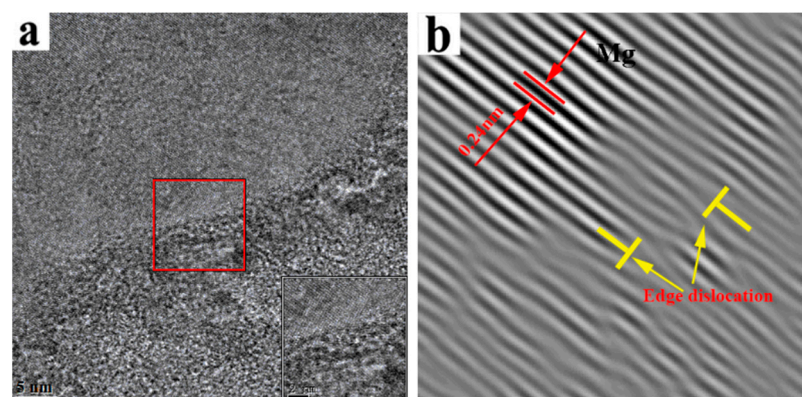


**Figure 14.** (a) HRTEM image of Grp/AZ91D interface; (b) the inverse FFT image of the area in the red box in (a).

Another strengthening mechanism is the Orowan looping mechanism. Under external force, the dislocation ring will be formed when the dislocations move to Grp. The bending degree of dislocation lines increases, which leads to an increase in dislocation movement resistance [21] and then improves the mechanical properties of materials.

When the mold temperature is low, most of the Grp is distributed at the grain boundary, and the strengthening mechanism is only a load transfer mechanism. With the increase in mold temperature, Grp tends to distribute in the interior of grains, which improves the strengthening effect of dislocation strengthening and the Orowan looping mechanism on the properties of composites. Based on the above analyses, the thixoforged Grp/AZ91D composite is strengthened by the synergistic effect of the load transfer, dislocation strengthening, and Orowan looping mechanism [22].

#### 4. Conclusions

- (1) When the holding temperature is 300 °C for 60 min, it is shown that an ideal semi-solid structure can be obtained. The appropriate semi-solid structure with grain size, shape fraction, and liquid fraction is 101.1 μm, 1.36, and 31.3%, respectively.
- (2) When the mold temperature reaches 300 °C, the excellent mechanical properties of the Grp/AZ91D composite are obtained. The UTS and elongation are 304.1 MPa and 13.9%, respectively. On the one hand, the amount of β phase decreases and the relative compactness of the SSSs increases with the increase in mold temperature. On the other hand, due to the self-stabilizing mechanism of Grp and its relationships with the solidifying interface, Grp could improve its mechanical properties by dispersion strengthening and fine-grain strengthening.
- (3) In comparison with the identical AZ91D alloy, the UTS and elongation of the thixoforged Grp/AZ91D composite increase by 11.1% and 43.1%, respectively. The excellent tensile properties of the thixoforged Grp/AZ91D composite are attributed to the strengthening of the Grp. The thixoforged Grp/AZ91D composite is strengthened by the synergistic effect of the load transfer, dislocation strengthening, and Orowan looping mechanism.

**Author Contributions:** Writing—original draft, S.Z., K.G., X.G. and H.J.; study design, S.Z., K.G., J.Z., J.W. and X.Z.; funding acquisition, S.Z. and J.Z.; writing—review and editing, S.Z., K.G., X.G., X.Z. and C.S.; data collection and analysis, K.G., X.G., S.Z., X.Z., H.J., J.W. and C.S. All authors have read and agreed to the published version of the manuscript.

**Funding:** The present work was funded by the Shandong Province Key Research and Development Plan (Grant NO. 2021SFGC1001, and Grant NO. 2021CXGC010310) and the Youth Innovation and Technology Support Program of Shandong Provincial Colleges and Universities (Grant No.2020KJA002), and Major innovation project for integrating science, education & industry of Qilu University of Technology (Shandong Academy of Sciences) (Grant No. 2022JBZ01-07).

**Data Availability Statement:** All data are available from the corresponding author on reasonable request.

**Conflicts of Interest:** The authors declare no conflict of interest.

#### References

1. Mordike, B.; Ebert, T. *Magnesium: Properties—Applications—Potential*; Elsevier: Amsterdam, The Netherlands, 2001.
2. Zhang, G.; Zhang, H.; Gao, M.; Wei, D. Mechanism of Effects of Rare Earths on Microstructure and Properties at Elevated Temperatures of AZ91 Magnesium Alloy. *J. Rare Earths* **2007**, *25*, 348–351. [[CrossRef](#)]
3. Yang, Y.; Xiong, X.; Chen, J.; Peng, X.; Chen, D.; Pan, F. Research advances in magnesium and magnesium alloys worldwide in 2020. *J. Magnes. Alloys* **2021**, *9*, 705–747. [[CrossRef](#)]
4. Velmurugan, V.; Mohan, B. Characterization and strengthening mechanism of CNT/TiB<sub>2</sub> particulates added AZ91D composites. *Mater. Res. Express* **2023**, *10*, 036504. [[CrossRef](#)]
5. Zhang, S.; Chen, T.; Cheng, F.; Li, L. Effects of mould temperature on microstructure and tensile properties of thixoforged Mg<sub>2</sub>Si p/AM60B in-situ composites. *J. Alloys Compd.* **2016**, *657*, 582–592. [[CrossRef](#)]
6. Guan, Z.-P.; Li, M.-Y.; Xia, K.-X.; Li, Z.-G.; Gao, D.; Zhao, P.; Ma, P.-K.; Song, J.-W. Microstructure, mechanical properties and wear resistance of SiCp/AZ91 composite prepared by vacuum pressure infiltration. *Trans. Nonferrous Met. Soc. China* **2022**, *32*, 104–121. [[CrossRef](#)]
7. Yang, K.; Zhang, F.; Chen, Y.; Zhang, H.; Xiong, B.; Chen, H. Recent progress on carbon-based composites in multidimensional applications. *Compos. Part A Appl. Sci. Manuf.* **2022**, *157*, 106906. [[CrossRef](#)]

8. Rashad, M.; Pan, F.; Hu, H.; Asif, M.; Hussain, S.; She, J. Enhanced tensile properties of magnesium composites reinforced with graphene nanoplatelets. *Mater. Sci. Eng. A* **2015**, *630*, 36–44. [[CrossRef](#)]
9. Gao, X.; Geng, K.; Sun, C.; Zhang, S.; Zhou, J.; Wu, J.; Zhang, X.; Wang, X. Effects of Graphite Particle Content and Holding Time on the Microstructure and Mechanical Properties of the Graphite/AZ91D Composite. *Metals* **2022**, *13*, 57. [[CrossRef](#)]
10. Aatthisugan, I.; Rose, A.; Jebadurai, D. Mechanical and wear behaviour of AZ91D magnesium matrix hybrid composite reinforced with boron carbide and graphite. *J. Magnes. Alloys* **2017**, *5*, 20–25. [[CrossRef](#)]
11. Chen, T.; Huang, L.; Huang, X.; Ma, Y.; Hao, Y. Effects of mould temperature and grain refiner amount on microstructure and tensile properties of thixoformed AZ63 magnesium alloy. *J. Alloys Compd.* **2013**, *556*, 167–177. [[CrossRef](#)]
12. Chen, T.; Ma, Y.; Wang, R.; Li, Y.; Hao, Y. Microstructural evolution during partial remelting of AM60B magnesium alloy refined by MgCO<sub>3</sub>. *Trans. Nonferrous Met. Soc. China* **2010**, *20*, 1615–1621. [[CrossRef](#)]
13. Dong, W.; Liu, Z.; Zhang, Y.; Quan, G. Effects of Semi-Solid Treatment Process Parameters on Microstructure of Extruded AZ91 Magnesium Alloy. *Rare Met. Mater. Eng.* **2014**, *43*, 2277–2280.
14. Chen, T.J.; Huang, L.K.; Huang, X.F.; Ma, Y.; Hao, Y. Effects of reheating temperature and time on microstructure and tensile properties of thixoformed AZ63 magnesium alloy. *Mater. Sci. Technol.* **2014**, *30*, 96–108. [[CrossRef](#)]
15. Okamoto, H.; Massalski, T. *Binary Alloy Phase Diagrams*; ASM International: Materials Park, OH, USA, 1990; Volume 3.
16. Boostani, A.; Mousavian, R.; Tahamtan, S.; Yazdani, S.; Khosroshahi, R.; Wei, D.; Xu, J.; Gong, D.; Zhang, X.; Jiang, Z. Graphene sheets encapsulating SiC nanoparticles: A roadmap towards enhancing tensile ductility of metal matrix composites. *Mater. Sci. Eng. A* **2015**, *648*, 92–103. [[CrossRef](#)]
17. Chen, L.; Xu, J.; Choi, H.; Pozuelo, M.; Li, X. Processing and properties of magnesium containing a dense uniform dispersion of nanoparticles. *Nature* **2015**, *528*, 539–543. [[CrossRef](#)] [[PubMed](#)]
18. Zhang, A.; Hao, H.; Zhang, X. Grain refinement mechanism of Al-5C master alloy in AZ31 magnesium alloy. *Trans. Nonferrous Met. Soc. China* **2013**, *23*, 3167–3172. [[CrossRef](#)]
19. Li, C.; Wang, X.; Liu, W.; Wu, K.; Shi, H.; Ding, C.; Hu, X.; Zheng, M. Microstructure and strengthening mechanism of carbon nanotubes reinforced magnesium matrix composite. *Mater. Sci. Eng. A* **2014**, *597*, 264–269. [[CrossRef](#)]
20. Erman, A.; Groza, J.; Li, X.; Choi, H.; Cao, G. Nanoparticle effects in cast Mg-1wt% SiC nano-composites. *Mater. Sci. Eng. A* **2012**, *558*, 39–43. [[CrossRef](#)]
21. Zhang, Z.; Chen, D. Consideration of Orowan strengthening effect in particulate-reinforced metal matrix nanocomposites: A model for predicting their yield strength. *Scr. Mater.* **2006**, *54*, 1321–1326. [[CrossRef](#)]
22. Li, P.; Cao, B.; Tan, W.; Gao, M. Microstructure and synergistic strengthening mechanisms of carbon nanotubes and Mg<sub>2</sub>Si nanoparticles hybrid reinforced Mg matrix composites prepared by powder thixoforming. *J. Alloys Compd.* **2020**, *818*, 152925. [[CrossRef](#)]

**Disclaimer/Publisher’s Note:** The statements, opinions and data contained in all publications are solely those of the individual author(s) and contributor(s) and not of MDPI and/or the editor(s). MDPI and/or the editor(s) disclaim responsibility for any injury to people or property resulting from any ideas, methods, instructions or products referred to in the content.